Summary

Summary goes here

Object and Measurement Models in X-ray CT

Rahul Singh

Anindya Bijoy Das

Aleksander Dogandžić

Iowa State University, USA

Abstract

Abstract goes here

Keywords: Computed Tomography, Image reconstruction.

Contents

Abbreviations **7**

Notations **9**

1 Introduction **11**
1.1 Section 1 11

2 Object Models **13**
2.1 Bruno De Man and Johan Nuyts Papers 13
2.1.1 Modeling of Linear Attenuation Coefficient 13
2.1.2 Summary 16
2.2 Charles Addison Bouman Papers 17
2.2.1 Modeling of Linear Attenuation Coefficient 17
2.2.2 Summary 20
2.3 Jeffrey A. Fessler Papers 21
2.3.1 Mono-energetic Model 21
2.3.2 Poly-energetic Model 22
2.3.3 Summary 26

3 Conclusion **27**

Appendices **29**

A Vectors and Matrices **31**

List of Tables

2.1 Photoelectric coefficient ϕ, Compton coefficient θ and monochromatic linear attenuation coefficient μ_{70keV} for a number of common substances 15
2.2 Coefficients of the Beam Hardening Function h used for pre-corrected data 20
2.3 Densities and water fractions of human tissues where the water fractions have been computed from a weighted least-squares fit to 2.58 25

List of Figures

2.1 Monochromatic linear attenuation coefficient μ_{70keV} versus ϕ (red) and θ (blue) (a) for various substances and (b) for the base substances (air, water, bone and Iron) only 16
2.2 Mass attenuation coefficients of various human tissues normalized at 40 keV 24
2.3 Water and bone fraction functions ($f_w(\rho) and f_b(\rho)$) computed using (a) displacement model; and (b) solution model 25

Abbreviations

ACC	Average Clustering Coefficient
APL	Average Path Length

Notations

G	An arbitrary graph
V	Set of vertices in a graph

Chapter 1

Introduction

1.1 Section 1

Intro goes here [1]

Chapter 2

Object Models

2.1 Bruno De Man and Johan Nuyts Papers

The research group of Bruno De Man and Johan Nuyts has a number of papers on the x-ray computed tomography. Among those, [2], [3] and [4] are some promising ones which can be quite helpful for reconstructing the conventional x-ray CT images, whereas [5] discusses about the reconstruction of helical CT images and [6] is a review paper on modeling the physics in the iterative reconstruction for transmission computed tomography. However, [4] is the most cited one and it is the extended version of [3] and [7]. It introduces a new algorithm-iterative maximum-likelihood (ML) polychromatic algorithm for computed tomography (IMPACT).

2.1.1 Modeling of Linear Attenuation Coefficient

The ultimate goal is to find the optimum distribution of linear attenuation coefficients $\{\mu_j\}_{j=1}^{J}$ from a given set of transmission measurements $\{y_i\}_{i=1}^{I}$, so that the following log-likelihood function is maximized.

$$L = \sum_{i=1}^{I} [\ y_i\ .\ ln(\widetilde{y}_i) - \widetilde{y}_i\ ] \tag{2.1}$$

where y_i is described as a Poisson realization of $\widetilde{y}_i$ for which the acquisition model is given by

$$\widetilde{y}_i = b_i\ .\ exp\left(-\sum_{j=1}^{J} l_{ij}\ .\ \mu_j\right) \tag{2.2}$$

where b_i is the number of photons that would be detected by detector i in the absence of absorber and measured by a calibration scan. On the other hand, l_{ij} is the effective intersection length of projection line i with pixel j and measured by the product of the interpolation coefficient and the row (or column) intersection length in the projection method. We know the step update equation for $\Delta\mu_j$ is

$$\Delta\mu_j \;=\; -\;\frac{\frac{\delta(L)}{\delta\mu_j}\,(\overrightarrow{\mu})}{\sum\limits_{h=1}^{J}\frac{\delta^2(L)}{\delta\mu_j\delta\mu_h}(\overrightarrow{\mu})} \tag{2.3}$$

Now, calculating the derivative and double derivative of L with respect to μ, we can find the updated μ after the n^{th} step, which is given by

$$\mu_j^{n+1} = \mu_j^n + \frac{\sum\limits_{i=1}^{I} l_{ij}\;.\;(\;\widetilde{y}_i\;-\;y_i\;)}{\sum\limits_{i=1}^{I} l_{ij}\;.\;\left[\;\sum\limits_{h=1}^{J} l_{ih}\;\right]\;.\;\widetilde{y}_i} \tag{2.4}$$

Now, the IMPACT algorithm considers a more general acquisition model which is given by

$$\widetilde{y}_i = \sum_{k=1}^{K} b_{ik}\;.\;exp\;\left(\;-\sum_{j=1}^{J}\;l_{ij}\;.\;\mu_{jk}\right) \tag{2.5}$$

where k is the energy index and K is the total number of energies. b_{ik} is the total energy detected by detector i in the absence of absorber for incident photons of energy E_k. Though, b_{ik} could be exploited to incorporate source fluctuation and the effect of the bow-tie filter, in this work, it is chosen to be independent and given by

$$b_{ik} \;=\; I_{ik}\;.\;S_k\;.\;E_k \tag{2.6}$$

The problem is that, now from 2.5, we have total $K \times J$ unknowns for the distribution of μ which would lead to poor convergence in comparison to 2.2 where we had only J unknowns. So, in this work, energy dependent linear attenuation coefficient $\mu(E)$ is approximated by a linear combination of a number of basic functions.

$$\mu(E) \;= a_1\;f_1(E)\;+\;a_2\;f_2(E)\;+ \ldots\;\ldots\;\ldots + a_n\;f_n(E) \tag{2.7}$$

The previous literature considers the energy dependence $\Phi(E)$ of the photoelectric effect and the energy dependence $\Theta(E)$ of Compton scatter as the basic functions of the linear attenuation coefficients [8], and thus the decomposition of $\mu_(E)$ is given by

$$\mu(E) \;= \phi\;.\;\Phi(E)\;+\;\theta\;.\;\Theta(E) \tag{2.8}$$

where ϕ is the photo-electric coefficient and θ is the Compton coefficient. Now the the energy dependence of the photo-electric effect and the Compton scatter is approximated by

$$\Phi(E) \;= \frac{1/E^3}{1/E_0^3} \tag{2.9}$$

$$\Theta(E) \;= \frac{f_{KN}(E)}{f_{KN}(E_0)} \tag{2.10}$$

where E_0 is a reference energy and $f_{KN}(E)$ is the Klein-Nishina function, given by

Substances	$\theta(1/cm)$	$\phi(1/cm)$	$\mu_{70keV}(1/cm)$
air	0.0002	1.7e-05	0.0002
soft tissue	0.1777	0.0148	0.1935
blood	0.1778	0.0154	0.1942
water	0.1793	0.0144	0.1946
muscle	0.1793	0.0155	0.2032
bone	0.3109	0.1757	0.4974
Ti	0.7189	1.8201	2.6536
Fe	1.3904	5.3273	7.0748

Table 2.1
Photoelectric coefficient ϕ, Compton coefficient θ and monochromatic linear attenuation coefficient μ_{70keV} for a number of common substances

$$f_{KN}(E) = \frac{1+\alpha}{\alpha^2} \cdot \left[\frac{2 \cdot (1+\alpha)}{1+2\alpha} - \frac{ln(1+2\alpha)}{\alpha} \right] + \frac{ln(1+2\alpha)}{2\alpha} - \frac{1+3\alpha}{(1+2\alpha)^2} \tag{2.11}$$

where $\alpha = E/511keV$.

Now, for any known substance we can know $\mu(E)$, and at any energy level, we can also know $\Phi(E)$ and $\Theta(E)$ from 2.9-2.11. Next, we can fit the least square method in 2.8 after discretization into K energy levels to find the values of the coefficients ϕ and θ. It is obvious that ϕ and θ actually represent the photoelectric part and the Compton scatter part of the attenuation at energy, $E = E_0 = 70keV$. Some calculated values are shown in Table 2.1 for some common substances. However, after discretizing 2.8, we get

$$\mu_{jk} = \phi_j \cdot \Phi_k + \theta_j \cdot \Theta_k \tag{2.12}$$

where Φ_k and Θ_k are known values representing the energy dependence of μ_{jk}; and ϕ_j and θ_j represent the material dependence and are unknown. However, the acquisition model of 2.5 becomes

$$\widetilde{y}_i = \sum_{k=1}^{K} b_{ik} \cdot exp \left(-\sum_{j=1}^{J} l_{ij} \cdot \phi_j \cdot \Phi_k - \sum_{j=1}^{J} \theta_j \cdot \Theta_k \right) \tag{2.13}$$

where the unknowns are $\{\phi_j\}_{j=1}^{J}$ and $\{theta_j\}_{j=1}^{J}$, so the number of unknowns are $2J$ instead of $K \times J$.

In this paper, some base substances have been considered, which are air, water, bone and iron. It is assumed that in the $\mu \sim \phi$ or $\mu \sim \theta$ graphs like in fig. 2.1a all the substances follow the piece-wise linear graphs which are created by the base-substances. It indicates that, at any pixel j, the coefficients can be written as the linear combination of the coefficients of the adjacent base-substances. Thus, for a given μ_j, we can use the piece-wise linear functions to find the photo-electric coefficients and Compton coefficients. It means that ϕ_j and θ_j can be substituted as $\phi(\mu_j)$ and $\theta(\mu_j)$ which leads the acquisition model to be like 2.14.

$$\widetilde{y}_i = \sum_{k=1}^{K} b_{ik} \cdot exp \left(-\Phi_k \sum_{j=1}^{J} l_{ij}\, \phi(\mu_j) \cdot - \Theta_k \sum_{j=1}^{J} l_{ij}\, \theta(\mu_j) \cdot \right) \tag{2.14}$$

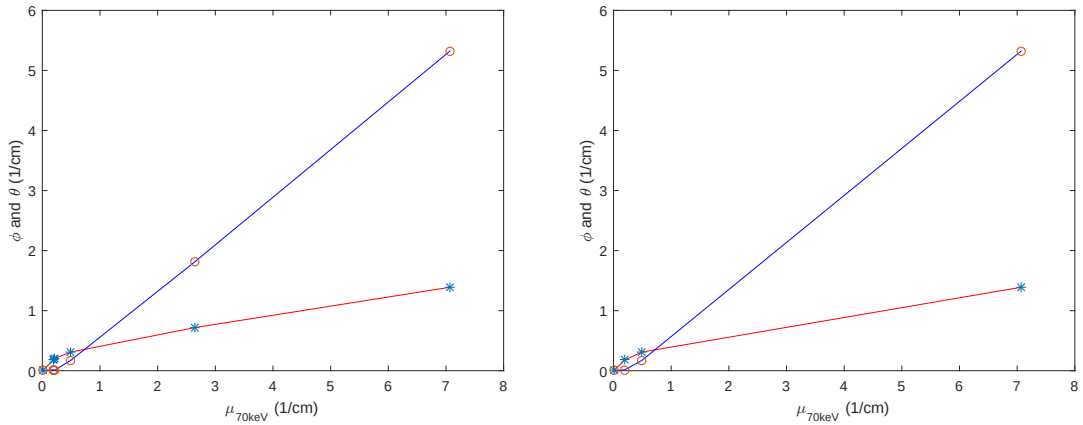

Figure 2.1: Monochromatic linear attenuation coefficient μ_{70keV} versus ϕ (red) and θ (blue) (a) for various substances and (b) for the base substances (air, water, bone and Iron) only

where $\phi(\mu_j)$ and $\theta(\mu_j)$ are known functions of μ_j which represents the monochromatic linear attenuation coefficient at $70keV$. Thus, the unknown is $\{\mu_j\}_{j=1}^{J}$, which means that the number of unknowns is J, as like as in 2.2. However, the update equation for $\{\mu_j\}_{j=1}^{J}$ can be derived using 2.3 and 2.14, which is given by-

$$\mu_j^{n+1} = \mu_j^n + \frac{\phi_j^{'} \cdot \sum_{i=1}^{I} l_{ij}\, c_i\, Y_i^{\Phi} \;+\; \theta_j^{'} \cdot \sum_{i=1}^{I} l_{ij}\, c_i\, Y_i^{\Theta}}{\phi_j^{'} \cdot \sum_{i=1}^{I} l_{ij}\, M_i \;+\; \sum_{i=1}^{I} l_{ij}\, N_i} \tag{2.15}$$

2.1.2 Summary

The key points of the previously described modeling of the linear attenuation coefficients in the IMPACT algorithm are presented below-

- This algorithm assumed the approximation of the energy dependent linear attenuation coefficients by a linear combination of basic functions corresponding to photoelectric effect and Compton scattering. Least square method has been applied to a previously available database to find the photo electric coefficients ϕ and Compton coefficients θ in 2.8.
- After observing the $\mu \sim \theta$ and $\mu \sim \phi$ graphs for various substances, four base substances have been chosen which are air, water, bone and iron and every pixel is assumed to contain a mixture of two adjacent base substances.
- This algorithm can deal with multiple materials/substances. At any energy index k, the energy dependence of photoelectric effect and Compton scattering can be found using 2.9-2.11. And, at any pixel j, the photoelectric coefficients and the Compton coefficients can be calculated using the graph in fig. 2.1b.

2.2 Charles Addison Bouman Papers

The research group of Charles Addison Bouman has also some very well-known papers on the reconstruction of X-ray CT images. Among those, [9] describes about the recent advancements of CT image reconstruction where he mentioned about two types of basic reconstruction approaches, which are analytical approaches and the iterative approaches. In [10], [11] and [12], the authors discuss mostly about the helical CT reconstructions. Now, we are actually going to discuss about the object and measurement modelling mentioned in [13] and [14].

2.2.1 Modeling of Linear Attenuation Coefficient

The received photon intensity of the i^{th} projection is denoted by y_i and is modeled as a Poisson random variable with the mean given by

$$\widetilde{y}_i = \mathbb{E}\left[y_i \mid \mu(\mathcal{E})\right] = \int_{\mathbb{R}} S_i(\mathcal{E}) \,.\, exp\left(-\sum_{j=1}^{J} l_{ij}\mu_j(\mathcal{E})\right) d\mathcal{E} \tag{2.16}$$

where $S_i(\mathcal{E})$ is the source-detector energy spectrum. For each projection, the standard log-converted CT projection [6] measurement Y_i is generated by

$$Y_i = -\, log\left(\frac{y_i}{\widetilde{b}_i}\right) \tag{2.17}$$

where $\widetilde{b}_i$ is the expected photon intensity in an air-calibration scan for the i^{th} projection, given by-

$$\widetilde{b}_i = \int_{\mathbb{R}} S_i(\mathcal{E})\, d\mathcal{E} \tag{2.18}$$

and then we can normalize the energy spectrum as $\widetilde{S}_i(\mathcal{E})$ given by

$$\widetilde{S}_i(\mathcal{E}) = \frac{S_i(\mathcal{E})}{\widetilde{b}_i} \tag{2.19}$$

It is assumed that $\widetilde{S}_i(\mathcal{E})$ is the same for all the projections, and that's why, the projection index i is dropped in $\widetilde{S}_i(\mathcal{E})$, and thus, from 2.17 it can be written that-

$$\widetilde{Y}_i = \mathbb{E}\left[Y_i \mid \mu(\mathcal{E})\right] = -\, log\left[\int_{\mathbb{R}} \widetilde{S}(\mathcal{E}) \,.\, exp\left(-\sum_{j=1}^{J} l_{ij}\mu_j(\mathcal{E})\right) d\mathcal{E}\right] \tag{2.20}$$

which is the conventional model for the non-linear beam hardening that results from a poly-energetic X-ray beam.

Now, the objective is to formulate a simple parametric model of the beam-hardening that occurs with a single, poly-chromatic scan of an object composed of two distinct materials, one with high density and the other with low. For doing this, a new variable is introduced as x_j which is defined by the weighted average of the linear attenuation coefficient of the j^{th} pixel with respect to the energy spectrum

$$x_j = \int_{\mathbb{R}} \widetilde{S}(\mathcal{E})\mu_j(\mathcal{E})\, d\mathcal{E} \tag{2.21}$$

which would help us to re-write the linear attenuation coefficient of the j^h pixel as

$$\mu_j(\mathcal{E}) = x_j r_j(\mathcal{E}) \tag{2.22}$$

where $r_j(\mathcal{E})$ is the absorption spectrum of the j^{th} pixel. So, we can write

$$r_j(\mathcal{E}) = \frac{\mu_j(\mathcal{E})}{\int_{\mathbb{R}} \widetilde{S}(\mathcal{E})\mu_j(\mathcal{E})\, d\mathcal{E}} \tag{2.23}$$

which indicates that the energy spectrum of r_j is normalized to 1, so for all j

$$\int_{\mathbb{R}} \widetilde{S}(\mathcal{E})r_j(\mathcal{E})\, d\mathcal{E} = 1 \tag{2.24}$$

Now, if the simple case is considered when the scanned object contains only one absorptive material denoted by $\mathcal{M}$, then $r_j(\mathcal{E})$ is identical for all pixels j, and we can write

$$\mu_j(\mathcal{E}) = x_j r_{\mathcal{M}} \tag{2.25}$$

where $r_{\mathcal{M}}$ is the absorption spectrum for the material $\mathcal{M}$. Thus, from 2.20, we can write the beam hardening function $f_{\mathcal{M}}(p_i)$ as

$$f_{\mathcal{M}}(p_i) = -\, log \left[\int_{\mathbb{R}} \widetilde{S}(\mathcal{E})\, .\, exp\left\{-r_{\mathcal{M}}(\mathcal{E})p_i\right\} d\mathcal{E} \right] \tag{2.26}$$

where p_i is the i^{th} projection given by

$$p_i = \sum_{j=1}^{J} l_{ij} x_j \tag{2.27}$$

and thus we can write

$$\widetilde{Y}_i = \mathbb{E}\left[Y_i \mid x\right] = f_{\mathcal{M}}(p_i) \tag{2.28}$$

Next, we can consider another case where the object is made of two different materials, one of low density and a second of high density. Here, the absorption spectrum $r_j(\mathcal{E})$ is modelled as a convex combination of two distinct absorption spectra given by

$$r_j(\mathcal{E}) = (1 - b_j)r_L(\mathcal{E}) + b_j r_H(\mathcal{E}) \tag{2.29}$$

where $r_L(\mathcal{E})$ and $r_H(\mathcal{E})$ represent the absorption spectrum of "low" and "high" density materials respectively, and b_j represents the fraction of material that is of high density for the j^{th} pixel. Using this model, the linear attenuation coefficient of the j^{th} pixel can be written as-

$$\mu_j(\mathcal{E}) = x_j \left[(1 - b_j)r_L(\mathcal{E}) + b_j r_H(\mathcal{E})\right] \tag{2.30}$$

In this work, only the binary case, i.e. $b_j \in \{0, 1\}$; is considered, so each pixel will be composed entirely of either low or high density materials. The value of b_j is directly estimated from the CT data as a part of the reconstruction process. So, from 2.20, it can be written that

$$\widetilde{Y}_i = \mathbb{E}\left[Y_i \mid \ x\right] = h\left(p_{L,i}, p_{H,i}\right) \tag{2.31}$$

which indicates that the expected projection measurement is now a non-linear function of two dimensional projections of the two materials where $h\left(p_{L,i}, p_{H,i}\right)$ is now a two dimensional beam hardening function given by

$$h\left(p_{L,i}, p_{H,i}\right) = -\ log\left[\int_{\mathbb{R}} \widetilde{S}(\mathcal{E})\ .\ exp\left\{-r_L(\mathcal{E})p_{L,i} - r_H(\mathcal{E})p_{H,i}\right\} d\mathcal{E}\right] \tag{2.32}$$

and $p_{L,i}$ and $p_{H,i}$ are the projections of the low and high density materials, respectively, given by

$$p_{L,i} = \sum_{j=1}^{J} l_{ij} x_j (1 - b_j) \tag{2.33}$$

$$p_{H,i} = \sum_{j=1}^{J} l_{ij} x_j b_j \tag{2.34}$$

Now the idea is to adaptively estimate this 2D beam hardening function during the reconstruction process. To do this, from some previous ideas that are available in the literature, the function is parameterized by a simple polynomial as

$$h\left(p_{L,i}, p_{H,i}\right) = \sum_{k=0}^{\infty} \sum_{l=0}^{\infty} \gamma_{k,l}\ \left(p_{L,i}\right)^k\ \left(p_{H,i}\right)^l \tag{2.35}$$

where $\gamma_{k,l}$ are the coefficients to be jointly estimated during the reconstruction, among which some of the first values can be calculated using 2.35. The model would be refereed as p^{th} ordered if the condition, $0 \leq k + l \leq p$, holds for all the unknown coefficients.

This two material beam-hardening model can also be used in the case when the projection measurement is pre-corrected for beam hardening of a single material. If the projection measurements have been pre-corrected with respect to the material $\mathcal{M}$ using the function $f_{\mathcal{M}}^{-1}$, then after the pre-correction, the expected projection measurement is approximately given by

$$\widetilde{Y}_i = \mathbb{E}\left[Y_i \mid x)\right] = \widetilde{h}\left(p_{L,i}, p_{H,i}\right) \tag{2.36}$$

where the 2D beam hardening function is given by

$$\widetilde{h}\left(p_{L,i}, p_{H,i}\right) = f_{\mathcal{M}}^{-1}\ .\ \left(-\ log\left[\int_{\mathbb{R}} \widetilde{S}(\mathcal{E})\ .\ exp\left\{-r_L(\mathcal{E})p_{L,i} - r_H(\mathcal{E})p_{H,i}\right\} d\mathcal{E}\right]\right) \tag{2.37}$$

. Thus using the same method as in 2.35, we can write-

$$\widetilde{h}\left(p_{L,i}, p_{H,i}\right) = \sum_{k=0}^{\infty} \sum_{l=0}^{\infty} \widetilde{\gamma}_{k,l}\ \left(p_{L,i}\right)^k\ \left(p_{H,i}\right)^l \tag{2.38}$$

where $\widetilde{\gamma}_{k,l}$ are the coefficients. In medical applications, it is common to pre-correct the projection measurements, Y_i, and this correction is usually based on a water phantom since human soft tissue is largely composed of water. Thus, here the pre-correction is given by $f_{\mathcal{M}}^{-1} = f_L^{-1}$ where f_L^{-1} is

index	$l=0$	l=1	l=2	$l=3$
$k=0$	0	1	$\widetilde{\gamma}_{0,2}$	$\widetilde{\gamma}_{0,3}$
$k=1$	1	$\widetilde{\gamma}_{1,1}$	$\widetilde{\gamma}_{1,2}$	$\widetilde{\gamma}_{1,3}$
$k=2$	0	$\widetilde{\gamma}_{2,1}$	$\widetilde{\gamma}_{2,2}$	$\widetilde{\gamma}_{2,3}$
$k=3$	0	$\widetilde{\gamma}_{3,1}$	$\widetilde{\gamma}_{3,2}$	$\widetilde{\gamma}_{3,3}$

Table 2.2
Coefficients of the Beam Hardening Function h used for pre-corrected data

the ideal beam hardening correction for the low density material. Thus, this pre-correction will linearize the low density measurement as

$$\widetilde{h}\left(p_{L,i},0\right)=f_{L}^{-1}\left(f_{L}(p_{L,i})\right)=p_{L,i} \tag{2.39}$$

which indicates that $\widetilde{\gamma}_{k,0}=0$ for $k\neq 1$, which are mentioned in table 2.2. Thus, for example, if a 3^{rd} order model ($p=3$) is considered, then $0\leq k+l\leq 3$, so there would be total five unknown coefficients for $\widetilde{\gamma}_{k,l}$ where $(k,l)\in\{(1,1),(2,1),(0,2),(1,2),(0,3)\}$.

Finally, if $y\in\mathbb{R}^{I}$ is the vector of the projection measurements, $x\in\mathbb{R}^{J}$ is the image vector, $b\in\{0,1\}^{J}$ be the vector of the material segmentation label mask, and $\gamma\in\mathbb{R}^{K}$ be the vector of fitting coefficients $\gamma_{k,l}$ (for a 3rd order model, K=5), then the formulation of the problem of simultaneous image reconstruction and beam hardening correction as the computation of maximum a posterior (MAP) estimate is given by-

$$\left\{\widehat{x},\widehat{b},\widehat{\gamma}\right\}=arg\ min_{x\geq 0,b,\gamma}\left\{-log\ \mathbb{P}(y\mid x,b,\gamma)-log\ \mathbb{P}(x,b)\right\} \tag{2.40}$$

where $\mathbb{P}(y\mid x,b,\gamma)$ is the likelihood function corresponding to X-ray forward model, and $\mathbb{P}(x,b)$ is the joint prior distribution over x and b.

2.2.2 Summary

The key points of the previously described method are mentioned below-

- This algorithm assumed that the object is formed by a combination of two distinct materials that can be separated based on their densities. A poly energetic X-ray forward model is formulated using a polynomial function of two material projections: one for the low density material and the other for the high.
- The linear attenuation coefficient is modeled as 2.30 where $r_L(\mathcal{E})$ and $r_H(\mathcal{E})$ represent the absorption spectrum of "low" and "high" density materials respectively, b_j represents the fraction of material that is of high density for the j^{th} pixel and x_j is described by 2.21.
- To obtain a multi-material beam hardening model, a simple polynomial has been considered in 2.35, where the coefficients of the polynomial are $\gamma_{k,l}$. Some of the first coefficients of γ are constant and pre-determined. The number of total coefficients depends on the approximation of the polynomial order considered for the experiment.
- The objective function is described in 2.40 where after the minimization of the objective value, along with the optimum image x, the optimum material segmentation mask b and the parameter vector γ, are also estimated.

2.3 Jeffrey A. Fessler Papers

The research group of Jeffrey A. Fessler has a number of very well-known papers on the iterative reconstruction of X-ray CT images too [15], [16], [17], [18], [19], [20], [21] and [22]. Among those, the processes of modeling of linear coefficients, mentioned in [18] and [19], are discussed here. The first one uses segmentation for the pixels whereas the later one does not.

2.3.1 Mono-energetic Model

First, the projection measurement y_i recorded by the ith detector would be given by-

$$y_i = I_i(\mathcal{E})\ exp\ \left\{ - \int_{L_i} \mu(x, y, z, \mathcal{E}) dl \right\} \tag{2.41}$$

whereas under the assumption of a mono-energetic model, the measurement simplifies to Beer's law

$$y_i = I_i(\mathcal{E}_0)\ exp\ \left\{ - \int_{L_i} \mu(x, y, z, \mathcal{E}_0) dl \right\} \tag{2.42}$$

where $\mu(x, y, z, \mathcal{E}_0)$ characterizes the overall attenuation property of an object which depends on the spatial coordinates (x, y, z) and $\mathcal{E}$, and has the units of inverse distance. The following statistical model has been assumed for the measurements-

$$y_i \ \sim \ Poisson\ \left\{ b_i e^{-[\mathbf{A}\mu]_i} \right\} \tag{2.43}$$

where $b_i = I_i(\mathcal{E}_0)$ is the black scan factor and N is the number of measured rays. The notation $[\mathbf{A}\mu]_i = \sum_{j=1}^{p} a_{ij}\mu_j$ represents the ith line integral and the $N \times p$ matrix $\mathbf{A} = \{a_{ij}\}$ is the system matrix which accounts for the system geometry as well as other significant physical effects such as detector response. For ray i and pixel j, a_{ij} is the area of overlap between the ray beam and the pixel, normalized by the detector width, and has units of length. The constants $\{b_i\}$ and $\{a_{ij}\}$ are non-negative and known.

Now to estimate the attenuation coefficient vector μ, the Poisson log-likelihood based estimation approach has been chosen which is given by

$$L(\mu) \ = \ \sum_{i=1}^{N} \left\{ y_i\ log \left(b_i e^{-[\mathbf{A}\mu]_i} \right) - \left(b_i e^{-[\mathbf{A}\mu]_i} \right) \right\} \tag{2.44}$$

When $\mathbf{A}$ has full column rank and the data is noise free, maximizing the likelihood would give a perfect result. In reality, the data is noisy and ML will give a very noisy reconstruction due to the ill-posedness of the problem, hence, regularization is needed here which is a penalty term that penalizes difference in the values of neighboring pixels and is given by

$$R(\mu) \ = \ \sum_{j=1}^{p} \sum_{k \in \mathcal{N}_j} \psi(\mu_j - \mu_k) \tag{2.45}$$

where $\mathcal{N}_j$ is some neighborhood of pixel j and ψ is a potential functions. The convex edge preserving Huber penalty is given by

$$f(x) = \begin{cases} \frac{x^2}{2}, & x \leq \delta \\ \delta \mid x \mid -\frac{\delta^2}{2}, & x \geqslant \delta \end{cases}$$

Combining the likelihood with a penalty gives the objective function

$$\Phi_1(\mu) = L(\mu) - \beta R(\mu) \tag{2.46}$$

where β is a scalar that controls the trade-off between the data-fit and the penalty terms. Now, the negative log-likelihood can be written as-

$$- \ L(\mu) = \sum_{i=1}^{N} g_i \left([\mathbf{A}\mu]_i \right) \tag{2.47}$$

where $g_i(l)$ is given by

$$g_i(l) = -Y_i log \left(b_i e^{-l} \right) + b_i e^{-l} \tag{2.48}$$

where a second-order Taylor's expansion to $g_i(l)$ around an estimate $\widehat{l_i}$ of the line integral yields

$$g_i(l) \approx g_i(\widehat{l_i}) + \dot{g}_i(\widehat{l_i})(l - (\widehat{l_i})) + \frac{\ddot{g}_i(\widehat{l_i})}{2}(l - \widehat{l_i})^2 \tag{2.49}$$

and now from 2.17 we can write about the estimate of the line-integral as-

$$\widehat{l_i} = log \left(\frac{b_i}{y_i} \right) \tag{2.50}$$

and utilizing this value, 2.49 gives the following approximation as

$$g_i(l) \approx (y_i - y_i log(y_i)) + \frac{y_i}{2}(l - \widehat{l_i})^2 \tag{2.51}$$

where the firsts term is independent of l, and thus, from 2.46 and 2.47, it can be written as

$$\Phi_2(\mu) = -\Phi_1(\mu) = \sum_{i=1}^{N} \frac{y_i}{2} \left([\mathbf{A}\mu]_i - \widehat{l_i} \right)^2 + \beta R(\mu) \tag{2.52}$$

Now, the goal of the reconstruction technique becomes to maximize $\Phi_1(\mu)$ or minimize $\Phi_2(\mu)$ subject to certain object constrains (such as non-negativity) which is represented mathematically by

$$\widehat{\mu} = \underset{\mu \geqslant 0}{arg\ max} \ \ \Phi_1(\mu) = \underset{\mu \geqslant 0}{arg\ min} \ \ \Phi_2(\mu) \tag{2.53}$$

2.3.2 Poly-energetic Model

The algorithm derived for the mono-energetic model ignores the poly-energetic nature of the x-ray beam and the energy dependence of the attenuation coefficient which results in non-linear beam hardening. It leads to a reduction in the reconstructed attenuation coefficient. For this reason, poly-energetic model has been introduced and an iterative reconstruction algorithm has been developed.

Pre-Segmented Model

It is assumed that the object is comprised of K known non-overlapping material types. For the k material type, the attenuation coefficient of the jth voxel is modeled by the product of the energy-dependent mass attenuation coefficient $m_k(\mathcal{E})$(known) and energy independent density ρ_j, which can be expressed as

$$\mu_j(\mathcal{E}) = \sum_{k=1}^{K} m_k(\mathcal{E}) \rho_j f_j^k(\rho_j) \tag{2.54}$$

where $f_j^k(\rho_j) = 1$ if the jth voxel belongs to the kth material type and $f_j^k(\rho_j) = 0$ otherwise. In this aspect, according to 2.16, the mean of the measured data along the path L is given by

$$\widetilde{y}_i = \mathbb{E}(y_i) = \int I_i(\mathcal{E}) \, . \, exp\left(- \sum_{j=1}^{p} \sum_{k=1}^{K} m_k(\mathcal{E}) \rho_j a_{ij} f_j^k(\rho_j) \right) d\mathcal{E} \tag{2.55}$$

Thus, using 2.44, we get the negative log-likelihood in the poly-energetic case as

$$-\, L(\rho) = \sum_{i=1}^{I} \; - \, y_i \, . \, ln(\widetilde{y}_i) + \widetilde{y}_i \tag{2.56}$$

which would be used in the following equation to get the optimum ρ.

$$\widehat{\rho} = \underset{\rho \geqslant 0}{arg\, max} \;\; \Phi_1(\rho) = \underset{\rho \geqslant 0}{arg\, min} \;\; \Phi_2(\rho) \tag{2.57}$$

Segmentation-Free Model

The difference between the pre-segmented model and the segmentation free model is that in the first case, the condition was f_j^k was equal to 0 or 1; but, now this tissue function can be fraction also. For simplicity, we just need to have $f_j^k(\rho_j) \geqslant 0$ and $\sum\limits_k f_j^k(\rho_j) = 1$ for all j.

From fig. 2.2, it can be seen that most of the soft tissues like ovary, brain, muscle, lung or blood, have spectral characteristics that are almost identical to those of water. Fat and breast tissue differ somewhat from water, and bone is significantly different. Because a soft tissues are spectrally similar to water, and have densities (0.95-1.06 g/cc) close to that of water, it is reasonable to use water as a base substance, and obviously, cortical bone is another natural choice for a base substance. The model could be augmented to include more base substances such as Iodine.

However, for bone and water, the attenuation coefficient of tissue is modeled as-

$$\mu_j(\mathcal{E}) \approx \left[m_w(\mathcal{E}) f_w^j(\rho_j) + m_b(\mathcal{E}) f_b^j(\rho_j) \right] \, . \, \rho_j \tag{2.58}$$

where $m_w(\mathcal{E})$ and $m_b(\mathcal{E})$ are the known mass attenuation coefficients of water and bone, respectively. The pixel tissue fraction functions f_w^j and f_b^j determine what extent the tissue in pixel j is spectrally water-like or bone-like, depending on the tissue density.

$$m(\mathcal{E}) = m_w(\mathcal{E}) \, f_w + m_b(\mathcal{E}) \, f_b \tag{2.59}$$

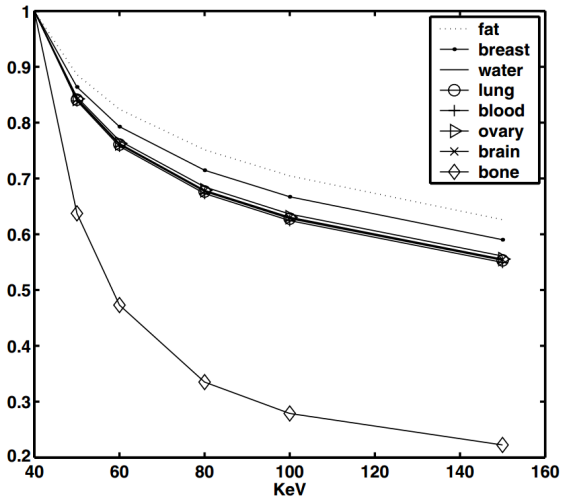

Figure 2.2: Mass attenuation coefficients of various human tissues normalized at 40 keV

Now the weighted least squares algorithm has been applied in the 2.58 to compute the coefficients f_w and f_b for the biological substances listed in fig. 2.2 imposing two more constraints. First, the solutions should be in the interval $[0, 1]$ and second, the sum of the solutions f_w and f_b would be unity. The results are listed in table 2.3 where it is observed that f_w is almost 1.0 for soft tissues and 0.0 for bone which confirms that the soft tissues are spectrally similar to water and water and bone can be used as distinct base substances. Now, in this paper, two models have been introduced to obtain the optimum solutions for $f_w(\rho)$ and $f_b(\rho)$.

Displacement Model includes the third-order polynomial functions shown in fig. 2.3a which have continuous first and second order derivatives and satisfy $f_w(\rho) + f_b(\rho) = 1$. This approach avoids the technical complications posed by the derivatives of piece-wise linear functions and has the potential for better accuracy, particularly for tissues that are spectrally similar to water , but have densities larger than water.

Solution Model assumes that the object contains a mineral solution in water (or some other solvent). In this model, the water-mineral solution density is greater than or equal to the density of water, and the attenuation coefficient can be modelled as

$$\mu(\mathcal{E}) \approx m_w(\mathcal{E})\rho_w + m_b(\mathcal{E})(\rho - \rho_w) = \rho \left[m_w(\mathcal{E})\frac{\rho_w}{\rho} + m_b(\mathcal{E})(1 - \frac{\rho_w}{\rho}) \right] \tag{2.60}$$

for $\rho \geq \rho_w$. The fraction function for this model are shown in fig. 2.3b, and are given by

$$f_w(\rho) = \begin{cases} 1, & \rho \leqslant \rho_w \\ \frac{\rho_w}{\rho}, & \rho \geq \rho_w \end{cases}$$

$$f_b(\rho) = \begin{cases} 0, & \rho \leqslant \rho_w \\ 1 - \frac{\rho_w}{\rho}, & \rho \geq \rho_w \end{cases}$$

where ρ_w is the density of water (or, more generally, the solvent). This model effectively assumes

Tissue	Density (g/cc)	f_w
Fat	0.95	1.00
Breast	1.02	1.00
Water	1.0	1.00
Lung	1.05	0.99
Blood	1.06	0.99
Ovary	1.05	0.99
Brain	1.04	0.99
Muscle	1.05	1.00
Eye lens	1.07	1.00
Testis	1.04	1.00
Cortical bone	1.92	0.00

Table 2.3
Densities and water fractions of human tissues where the water fractions have been computed from a weighted least-squares fit to 2.58

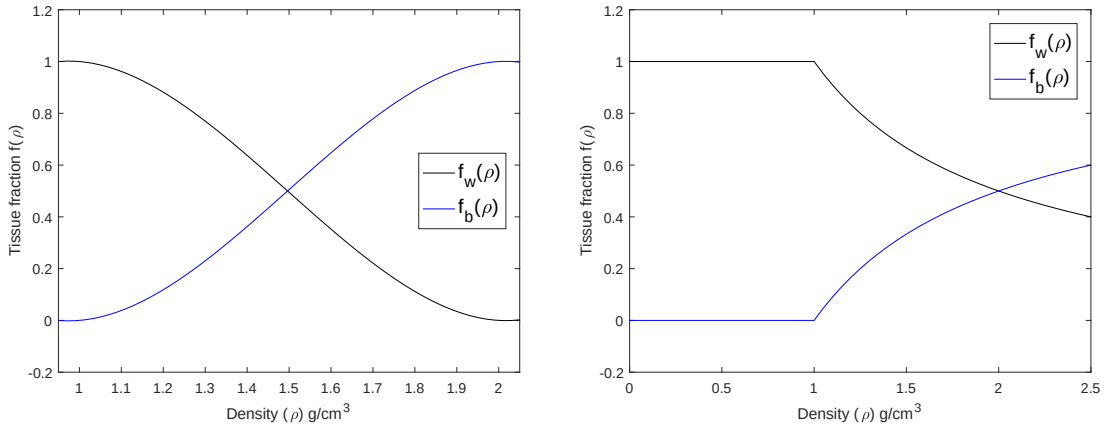

Figure 2.3: Water and bone fraction functions ($f_w(\rho) and f_b(\rho)$) computed using (a) displacement model; and (b) solution model

that the object consists of water everywhere whose density has increased because of mineral content. It is shown in this paper that this solution model has performed better than the displacement model.

2.3.3 Summary

The key points of the previously described method are mentioned below-

- This algorithm assumed that the object can be formed by a combination of multiple materials where a mono-energetic and a poly-energetic X-ray model are formulated.
- The linear attenuation coefficient is modeled as the product of the energy-dependent mass attenuation coefficient $m_k(\mathcal{E})$(known) and energy independent density ρ_j, which is described in 2.54.
- A tissue fraction function f_j^k has been introduced which can have values of only 0 and 1 in the pre-segmented case and can have fraction values in the segmentation-free case. Two models have been described about the procedure of obtaining the values of the fraction, and it is mentioned that solution model performs better than the displacement model in the segmentation free case. In both of the cases, water and bone have been considered as the base substances.
- The objective function is described in 2.52 where $L(\mu)$ is the log likelihood function and $R(\mu)$ is the regularization penalty, and thus the optimum μ (mono-energetic case) or the optimum ρ (poly-energetic case) is calculated using 2.53 or 2.57, respectively.

Chapter 3

Conclusion

Appendices

Appendix A

Vectors and Matrices

Bibliography

[1] R. Gu and A. Dogandžić, "Blind x-ray ct image reconstruction from polychromatic poisson measurements," *IEEE Transactions on Computational Imaging*, vol. 2, no. 2, pp. 150–165, 2016.

[2] B. De Man, J. Nuyts, P. Dupont, G. Marchal, and P. Suetens, "Metal streak artifacts in x-ray computed tomography: a simulation study," *IEEE Transactions on Nuclear Science*, vol. 46, no. 3, pp. 691–696, 1999.

[3] ——, "Reduction of metal streak artifacts in x-ray computed tomography using a transmission maximum a posteriori algorithm," *IEEE transactions on nuclear science*, vol. 47, no. 3, pp. 977–981, 2000.

[4] ——, "An iterative maximum-likelihood polychromatic algorithm for ct," *IEEE transactions on medical imaging*, vol. 20, no. 10, pp. 999–1008, 2001.

[5] J. Nuyts, B. De Man, P. Dupont, M. Defrise, P. Suetens, and L. Mortelmans, "Iterative reconstruction for helical ct: a simulation study," *Physics in medicine and biology*, vol. 43, no. 4, p. 729, 1998.

[6] J. Nuyts, B. De Man, J. A. Fessler, W. Zbijewski, and F. J. Beekman, "Modelling the physics in the iterative reconstruction for transmission computed tomography," *Physics in medicine and biology*, vol. 58, no. 12, p. R63, 2013.

[7] J. Nuyts, P. Dupont, and L. Mortelmans, "Iterative reconstruction of transmission sinograms with low signal to noise ratio," in *2nd IEEE Workshop CMP: can we beat the curse of dimensionality (Prague, Czech Republic, Aug. 28-30, 1996)*, 1997, pp. 237–248.

[8] D. E. Avrin, A. Macovski, and L. M. Zatz, "Clinical application of compton and photo-electric reconstruction in computed tomography: preliminary results." *Investigative radiology*, vol. 13, no. 3, pp. 217–222, 1978.

[9] J. Hsieh, B. Nett, Z. Yu, K. Sauer, J.-B. Thibault, and C. A. Bouman, "Recent advances in ct image reconstruction," *Current Radiology Reports*, vol. 1, no. 1, pp. 39–51, 2013.

[10] J.-B. Thibault, K. D. Sauer, C. A. Bouman, and J. Hsieh, "A three-dimensional statistical approach to improved image quality for multislice helical ct," *Medical physics*, vol. 34, no. 11, pp. 4526–4544, 2007.

[11] Z. Yu, J.-B. Thibault, C. A. Bouman, K. D. Sauer, and J. Hsieh, "Fast model-based x-ray ct reconstruction using spatially nonhomogeneous icd optimization," *IEEE Transactions on image processing*, vol. 20, no. 1, pp. 161–175, 2011.

[12] S. Venkatakrishnan, L. Drummy, M. Jackson, C. Bouman, J. Simmons, and M. De Graef, "A phantom-based forward projection approach in support of model-based iterative reconstructions for haadf-stem tomography," *Ultramicroscopy*, vol. 160, pp. 7–17, 2016.

[13] P. Jin, C. A. Bouman, and K. D. Sauer, "A model-based image reconstruction algorithm with simultaneous beam hardening correction for x-ray ct," *IEEE Transactions on Computational Imaging*, vol. 1, no. 3, pp. 200–216, 2015.

[14] R. Zhang, J.-B. Thibault, C. A. Bouman, K. D. Sauer, and J. Hsieh, "Model-based iterative reconstruction for dual-energy x-ray ct using a joint quadratic likelihood model," *IEEE transactions on medical imaging*, vol. 33, no. 1, pp. 117–134, 2014.

[15] H. Erdogan and J. A. Fessler, "Ordered subsets algorithms for transmission tomography," *Physics in medicine and biology*, vol. 44, no. 11, p. 2835, 1999.

[16] ——, "Monotonic algorithms for transmission tomography," in *Biomedical Imaging, 2002. 5th IEEE EMBS International Summer School on.* IEEE, 2002, pp. 14–pp.

[17] I. A. Elbakri and J. A. Fessler, "Statistical x-ray-computed tomography image reconstruction with beam-hardening correction," in *Medical Imaging 2001.* International Society for Optics and Photonics, 2001, pp. 1–12.

[18] ——, "Statistical image reconstruction for polyenergetic x-ray computed tomography," *IEEE transactions on medical imaging*, vol. 21, no. 2, pp. 89–99, 2002.

[19] ——, "Segmentation-free statistical image reconstruction for polyenergetic x-ray computed tomography with experimental validation," *Physics in medicine and biology*, vol. 48, no. 15, p. 2453, 2003.

[20] S. Srivastava and J. A. Fessler, "Simplified statistical image reconstruction algorithm for polyenergetic x-ray ct," in *IEEE Nuclear Science Symposium Conference Record*, vol. 3. Citeseer, 2005, pp. 1551–1555.

[21] M. Abella and J. A. Fessler, "A new statistical image reconstruction algorithm for polyenergetic x-ray ct," in *2009 IEEE International Symposium on Biomedical Imaging: From Nano to Macro.* IEEE, 2009, pp. 165–168.

[22] J. A. Fessler and H. Erdogan, "A paraboloidal surrogates algorithm for convergent penalized-likelihood emission image reconstruction," in *Nuclear Science Symposium, 1998. Conference Record. 1998 IEEE*, vol. 2. IEEE, 1998, pp. 1132–1135.